
Dual-Side Feature Fusion 3D Pose Transfer

Jue Liu¹, Feipeng Da^{1*}

¹The School of Automation, Southeast University, China.
{liu_jue,dafp}@seu.edu.cn

Abstract

3D pose transfer solves the problem of additional input and correspondence of traditional deformation transfer, only the source and target meshes need to be input, and the pose of the source mesh can be transferred to the target mesh. Some lightweight methods proposed in recent years consume less memory but cause spikes and distortions for some unseen poses, while others are costly in training due to the inclusion of large matrix multiplication and adversarial networks. In addition, the meshes with different numbers of vertices also increase the difficulty of pose transfer. In this work, we propose a *Dual-Side Feature Fusion Pose Transfer Network* to improve the pose transfer accuracy of the lightweight method. Our method takes the pose features as one of the side inputs to the decoding network and fuses them into the target mesh layer by layer at multiple scales. Our proposed *Feature Fusion Adaptive Instance Normalization* has the characteristic of having two side input channels that fuse pose features and identity features as denormalization parameters, thus enhancing the pose transfer capability of the network. Extensive experimental results show that our proposed method has stronger pose transfer capability than state-of-the-art methods while maintaining a lightweight network structure, and can converge faster. Code is available at <https://github.com/YikiDragon/FF-PTNet>.

1 Introduction

3D pose transfer is gradually becoming a research hotspot in the field of computer graphics and vision. It was derived from deformation transfer in the past, and it has been proven to be superior after extensive research. Previous deformation transfer methods often relied on additional inputs, such as correspondence between vertices [22], skeleton and weight information [9], auxiliary meshes [27], and key point annotations [2], which are often difficult to obtain in practical applications. For this reason, Wang et al. first proposed the concept of Neural Pose Transfer (NPT) [25], its core idea is to transfer the identity features of the target to the source mesh through the SPAdaIN module instead of transferring the pose features to the target mesh, for which the forward propagation in the SPAdaIN module mixes the target vertices and the pose code, while the side input direction is the target vertices. This may result in the network not being able to transfer some unseen poses. In addition, the origin model of NPT cannot perform the task of pose transfer between meshes with different numbers of vertices because it needs to encode the pose features into the same dimension as the source mesh vertices. While the maxpool model, although the output mesh is not as smooth as the origin model, can adapt to meshes with the different number of vertices, and also proves that a fixed-length pose code can effectively express the pose features.

Through the above analysis, we propose a 3D pose transfer method based on dual-side feature fusion (*FF-PTNet*), which can transfer the pose of the source mesh while well preserving the identity details of the target mesh. Some examples of our methods are shown in the Figure 1. In this work, our

*Corresponding author at: The School of Automation, Southeast University, Nanjing, Jiangsu, 210096, China.

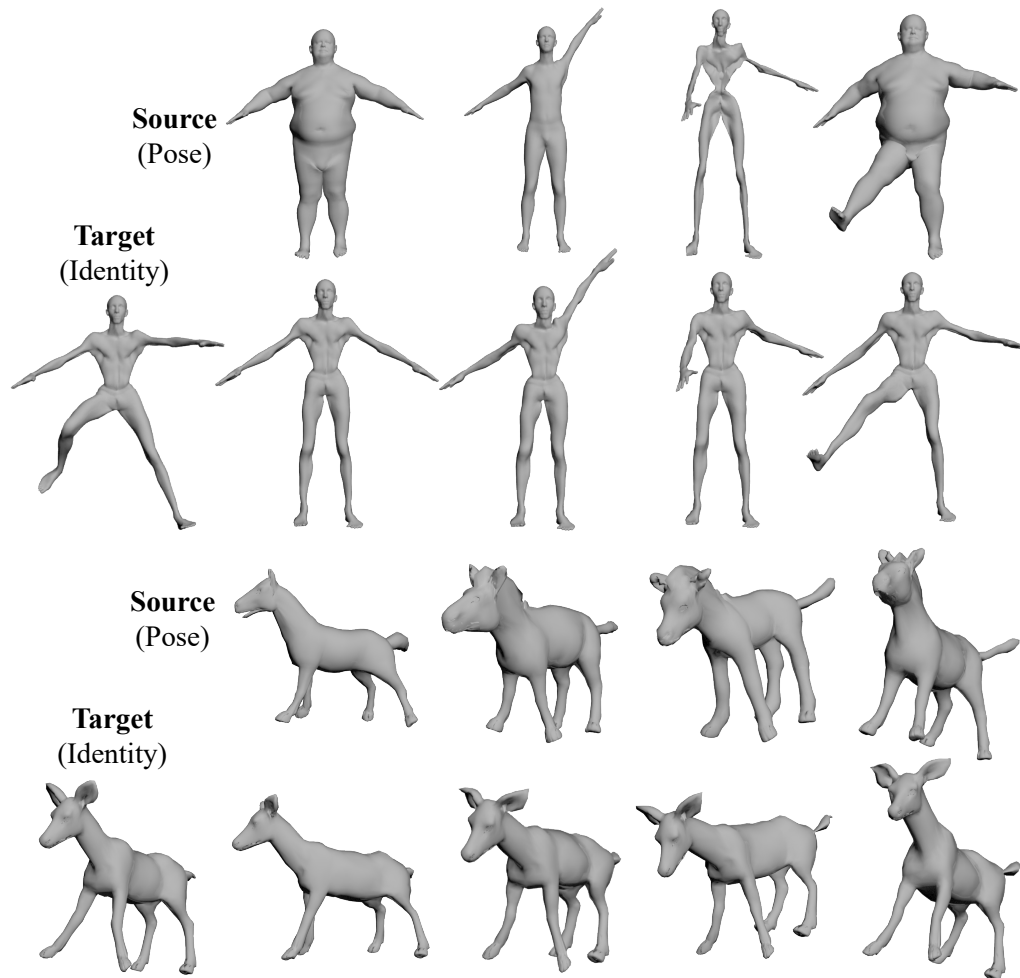


Figure 1: **The results of our *FF-PTNet* for pose transfer.** "Source" and "Target" are the customary representations in Deformation transfer. In the top two rows are the human identity and pose from SMPL [17], and in the bottom two rows are the animal identity and pose from SMAL [30].

proposed *Feature Fusion Adaptive Instance Normalization (FFAdaIN)* contains two side inputs: the mixed features and the target vertices. We adopt this design scheme because after several experiments, we found that appropriately adding pose code to the side input of the conditional normalization module can effectively improve the pose transfer performance of the model, and keeping the target mesh of the side input can make the output mesh smoother. In addition, We also tried to incorporate multi-scale pose features into the target mesh and found in our experiments that this resulted in more refined deformation effects.

Contributions We propose to input both identity and pose features in the side channel of the conditional normalization module and propose a new mesh decoder structure that fuses identity and pose features layer by layer to preserve as much detail as possible. Extensive experiments show that our method outperforms state-of-the-art methods in both qualitative and quantitative terms. To the best of our knowledge, our method is the first to use pose features for conditional normalized side-channel input and achieves more accurate pose transfer effects and faster training of the network.

2 Related work

2.1 Deformation transfer

3D pose transfer is derived from the 3D deformation transfer. Sumner et al. first proposed the classical deformation transfer algorithm (DT) [22], which represents the deformation process between meshes by a sparse matrix, and transforms the reference mesh into a shape similar to the target mesh by least squares, then generates a correspondence between the source and target meshes, after which the similar least squares method is applied to transfer the deformation to the target mesh. Ben-Chen et al. first proposed to apply deformation not directly to the model, but to the spatial region wrapping the model, which is also called the "cage" method [2]. "Cage" was constructed by the Poisson surface reconstruction method [13] and used to control the point cloud of its wrapping. In recent years, Yifan et al. proposed a deep learning-based "cage" generation method [28], which converts a spherical mesh into a "cage" for the source and target meshes respectively, and then builds cage and mesh mappings using MVC function [11] so that the "cage" of the source mesh can be applied to the target mesh for deformation transfer. Sung et al. proposed to use vectors in the latent space to encode the deformation [23] and then combine the shape features of the point cloud for decoding to obtain the final point cloud. Liao et al. proposed to predict the skinning weights of the mesh using a graph convolution model [15] and calculate the transformation matrix of each part of the mesh using the ICP alignment algorithm [3], and finally obtain the final mesh using the LBS algorithm [12].

2.2 Pose transfer

3D pose transfer is a very challenging 3D reconstruction task. Wang et al. first introduced the concept of Neural Pose Transfer (NPT) [25], and their SPAdaIN module, inspired by the 2D image style transfer method, can transfer the shape style of the target mesh to the source mesh. Song et al. proposed 3D-CoreNet [20; 21], It proposed ElaIN for mesh refinement while using optimal transport methods to solve the correspondence between source and target meshes. Chen et al [7] used GAN to solve the pose transfer problem, which refers to the idea of multi-feature decoupling of 2D images [14] and encodes the mesh into intrinsic and extrinsic feature codes through an encoder, where the intrinsic and extrinsic feature codes represent identity and pose respectively, and converting the combined feature code to a mesh by a generator. A similar idea is also reflected in the work of Armstrong et al [1], which encodes the point cloud into intrinsic features, extrinsic features, and rotation features, and the pose of the reconstructed point cloud can be controlled by extrinsic feature codes.

2.3 Arbitrary style transfer and semantic image synthesis

Many researchers have proposed various methods to achieve arbitrary style transfer. A typical method for arbitrary style transfer is AdaIN [10], which is based on the improvement of InstanceNorm [24]. AdaIN uses the mean and variance of each channel of the style image to denormalize the normalized image to achieve style transfer. The AdaConv module was proposed to extend AdaIN to enable it to extract local features in the style images and thus output more detailed images [6]. Liu et al. proposed adding an attention mechanism to AdaIN [16], which slightly improves the accuracy and generalization of the model but also requires a lot of memory for training.

Semantic image synthesis is an important research direction in the field of computer vision. Some classical CNN-based methods include CRN [8], pix2pixHD [26], SIMS [19], and SPADE [18]. SPADE designed three convolution layers to extract the features of the semantic map to denormalize the data after batchnorm [18] to obtain the synthetic image, but only the semantic map is used in the denormalization process and the style features of the source image are ignored. Zhu et al. proposed SEAN to add encoding of style features of the source image and design two learnable parameters to do a weighted summation of style and semantic features so that the synthesized image retains the style of the source image well [29]. Our method is highly inspired by SEAN.

3 Method

The 3D mesh pose transfer problem can be described as follows: Define a 3D mesh as $M(I, P)$, where I represents the identity of the mesh (e.g., man, woman), P is the pose of this mesh. The

purpose of 3D mesh pose transfer is to input the source $M(I_{src}, P_{src})$ and target $M(I_{tgt}, P_{tgt})$ and then compute the output mesh $\hat{M}(I_{tgt}, P_{src})$ with the source mesh pose and target mesh identity. During our experiments with previous methods, we found that the pose transfer method based on style transfer [25] lacks the preservation of the target mesh details and the generated mesh also suffers from spikes and artifacts. Then the optimal transport-based methods [20; 21] can achieve the mesh pose transfer with different numbers of vertices, but such methods consume a lot of memory and also seriously slow down the running speed due to the existence of large matrix multiplication. Finally, the GAN-based method [7] also relies on high-performance computers for training and it cannot adapt to pose transfer with different numbers of vertices. By experimenting and summarizing the above methods, we propose an idea that the accuracy of pose transfer might be improved if the pose features of the source mesh and the identity features of the target mesh are fused first, and then the fused features are used for multi-scale denormalization.

Therefore, we designed the *Dual-Side Feature Fusion Pose Transfer Network (FF-PTNet)*, and the network architecture is shown in Figure 2. The network mainly consists of a pose encoder and three residual blocks, where the residual blocks consist of two *Feature Fusion Adaptive Instance Normalization (FFAdaIN)*. FFAdaIN is a major innovation of this paper, which greatly improves the convergence speed, accuracy, and robustness of the pose transfer model. Further details of our FF-PTNet are described below.

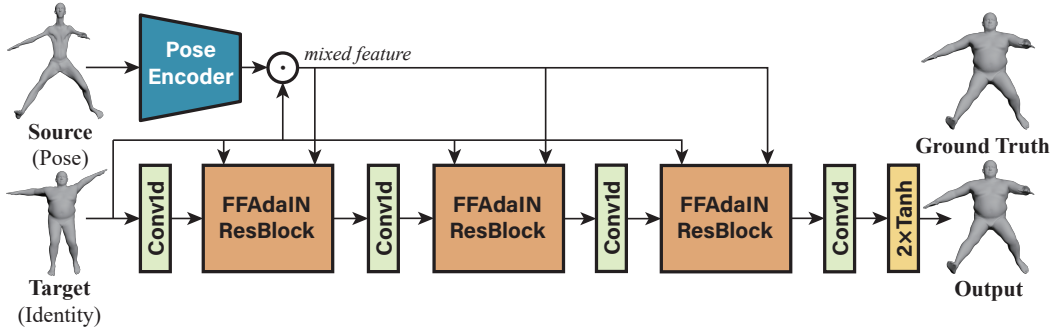


Figure 2: **The overall architecture of our FF-PTNet.** With $M(I_{src}, P_{src})$ and $M(I_{tgt}, P_{tgt})$ as inputs, the pose code z_{po} is extracted from $M(I_{src}, P_{src})$ by Pose Encoder. The decoding structure generates $\hat{M}(I_{tgt}, P_{src})$ guided by z_{po} . The symbol \odot denotes the concatenation operation.

3.1 FFAdaIN

The detailed architecture of FFAdaIN is shown in Figure 3 (b), where the vertical direction is the forward propagation direction of FFAdaIN. To import pose features in denormalization, our FFAdaIN module contains two side inputs: the vertices of target mesh v_{id} and the mixed feature f_{mix} , which is obtained from v_{id} and the pose code z_{po} after concatenation operation. In our method, z_{po} is a vector of length 1024, which cannot be concatenated directly with v_{id} of size $N \times 3$. Therefore, it is necessary to repeat z_{po} into a size of $N \times 1024$. Then the size of f_{mix} is constructed as $N \times 1027$. This design allows our method to be used for meshes with different numbers of vertices.

The FFAdaIN module is designed with four convolution layers and two learnable parameters α and β . The convolution layers extract two pairs of feature variables γ_{id}, δ_{id} and $\gamma_{mix}, \delta_{mix}$ from v_{id} and f_{mix} , respectively. α and β are automatically adjusted during training to find the optimal proportion of pose and identity feature fusion. The denormalization parameters γ_{ff} and δ_{ff} are computed by weighted summation of $\gamma_{id}, \gamma_{mix}$ and $\delta_{id}, \delta_{mix}$ by α and β , respectively. The input activation values h_{input} are normalized channel-by-channel and then denormalized using γ_{ff} and δ_{ff} to obtain the output. The output of FFAdaIN is computed as follows, where μ_{input} and σ_{input} are the mean and standard deviation of the input activation values on each channel:

$$\begin{aligned} \gamma_{id} &= \text{Conv1d}_{id1}(v_{id}) & \gamma_{mix} &= \text{Conv1d}_{mix1}(f_{mix}) \\ \delta_{id} &= \text{Conv1d}_{id2}(v_{id}) & \delta_{mix} &= \text{Conv1d}_{mix2}(f_{mix}) \end{aligned} \quad (1)$$

$$\begin{aligned}\gamma_{ff} &= \alpha\gamma_{id} + (1 - \alpha)\gamma_{mix} \\ \delta_{ff} &= \beta\delta_{id} + (1 - \beta)\delta_{mix}\end{aligned}\quad (2)$$

$$FFAdaIN(h_{input}, f_{mix}, v_{id}) = \gamma_{ff} \frac{(h_{input} - \mu_{input})}{\sigma_{input}} + \delta_{ff} \quad (3)$$

The design of SPAdaIN ResBlock in NPT [25] contains 3 SPAdaIN units, and we found during our experiments that removing any one of the SPAdaIN units would cause the model to fail to converge to the desired range. In contrast, we designed FFAdaIN to enhance the feature fusion capability from the side input, so the FFAdaIN ResBlock is designed as in Figure 3 (c), and using only 2 FFAdaIN units makes our network exceed the NPT in performance and not much larger than the NPT in size.

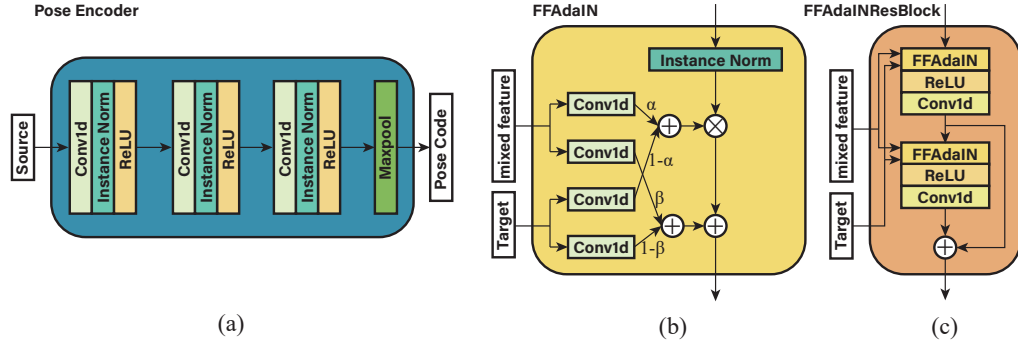


Figure 3: **Detailed architecture of network components.** (a) Pose encoder architecture, (b) FFAdaIN architecture and (c) FFAdaIN Resblock architecture.

3.2 Pose Encoder

The detailed architecture of the pose encoder is shown in Figure 3 (a), where we follow the design of NPT [25] but use a maxpool layer to extract feature vectors as pose code z_{po} in the output. Since the pose features in our model are input from the side of the FFAdaIN module and do not need to go through the InstanceNorm, it is feasible to use one-dimensional feature vectors. In addition, the two models provided by NPT show that the one-dimensional pose code obtained by the maxpool method is enough to express the pose features. Taking a source mesh with vertices size of $N \times 3$ as an example, the pose encoder consists of three one-dimensional convolution units with a kernel size of 1×1 . The size of the first dimension of each unit output is kept as N while the second dimension increases layer by layer, and the feature size of the last convolution unit output is $N \times 1024$. Finally, the pose code z_{po} with length 1024 is extracted through a maxpool layer.

3.3 Loss function

We optimize our network by minimizing the following loss function.

Reconstruction Loss Following most previous approaches [25; 20; 7; 21], we use reconstruction loss for supervised training of the network. This loss function requires that the prediction mesh output by the network has a correspondence with the ground truth mesh. Since the prediction mesh is obtained from the target mesh by pose transfer, these two meshes have a correspondence, so we make the vertices of ground truth also sorted according to the target mesh. The reconstruction loss is computed as follows, where N is the number of vertices, x_{pred} and x_{gt} are the coordinates of the vertices of the prediction mesh and ground truth mesh, respectively.

$$L_{rec} = \frac{1}{N} \sum_{i=1}^N \|x_{pred} - x_{gt}\|_2^2 \quad (4)$$

Edge Length Constraint The edge length constraint is used to avoid large edge length variations during pose transfer and to make the prediction mesh smoother. Unlike previous methods [25; 20; 21] we believe that the use of prediction mesh and ground truth mesh as input to the loss function can lead to better effect. The edge length constraint is computed as follows, where E is the number of edges, and l_{pred} and l_{gt} are the edge lengths of the prediction mesh and ground truth mesh, respectively.

$$L_{edg} = \frac{1}{E} \sum_{e=1}^E |l_{pred}/l_{gt} - 1| \quad (5)$$

We optimize the model using the combined loss function, where the value of λ is chosen to be 0.0005.

$$L = L_{rec} + \lambda L_{edg} \quad (6)$$

4 Experiment

Datasets We choose the human mesh generated in NPT [25] based on SMPL [17] for training and validating the human pose transfer network. The training set contains 16 identities and 400 poses. 6400 pairs (source and target lattices) are used as an epoch, where each pair of meshes is chosen randomly and the vertices are shuffled. The corresponding ground truth is also selected according to the source mesh’s pose and the target mesh’s identity. Before feeding into the network, The center of the mesh is moved to the origin according to the bounding box of the mesh and the coordinates are scaled according to the longest edge of the bounding box so that all coordinate values are between -1 and 1. The validation set contains 14 identities and 800 poses (including the same 400 poses as the training set and another 400 poses). The source and target meshes are also randomly selected and their vertices are shuffled during the validation process, and the seen and unseen poses are validated separately. In addition to training the pose transfer network for animal meshes, we also choose the animal meshes generated in 3D-CoreNet [20] based on SMAL [30] as training and validation data. The training set contains 24 identities and 300 poses, and the training process uses 7200 pairs of meshes as an epoch. The validation set contains 16 identities and 600 poses, and the preprocessing is the same as the human meshes.

Implementation details We use the AdamW optimizer to train the model with an initial learning rate of 1e-3 and then decay at a rate of 0.8 after every 8 epochs, for a total of 200 epochs. The batch size was set to 8 during training, and an RTX 3080 12G GPU was used for training.

Evaluation metrics We evaluate the model using the classical Point-wise Mesh Euclidean Distance (PMD), and obtain the PMD value by computing the average $L2$ distance between the vertices of predicted mesh and ground truth mesh.

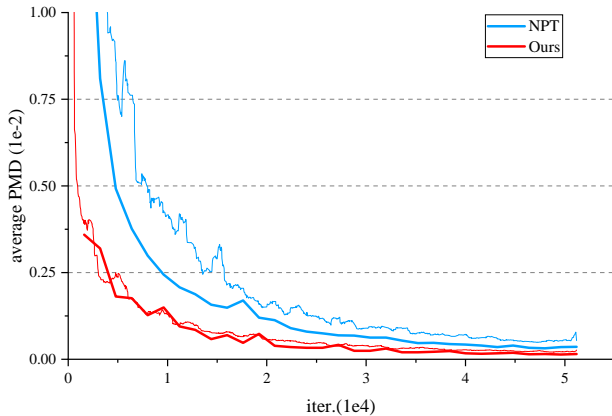


Figure 4: **Training on SMPL.** Thin curves are training error per iteration and bold curves are validation error per epoch.

4.1 Training Comparison

We chose NPT [25] to compare with our method for the training process. As Figure 4 records the average PMD curves of NPT [25] and our *FF-PTNet* during 51,200 iterations, the thin curves are the error of each iteration during training, and the bold curves are the validation error of one epoch. Our method converges much faster than NPT, and the training and validation errors at the end of the iteration are significantly smaller than NPT.

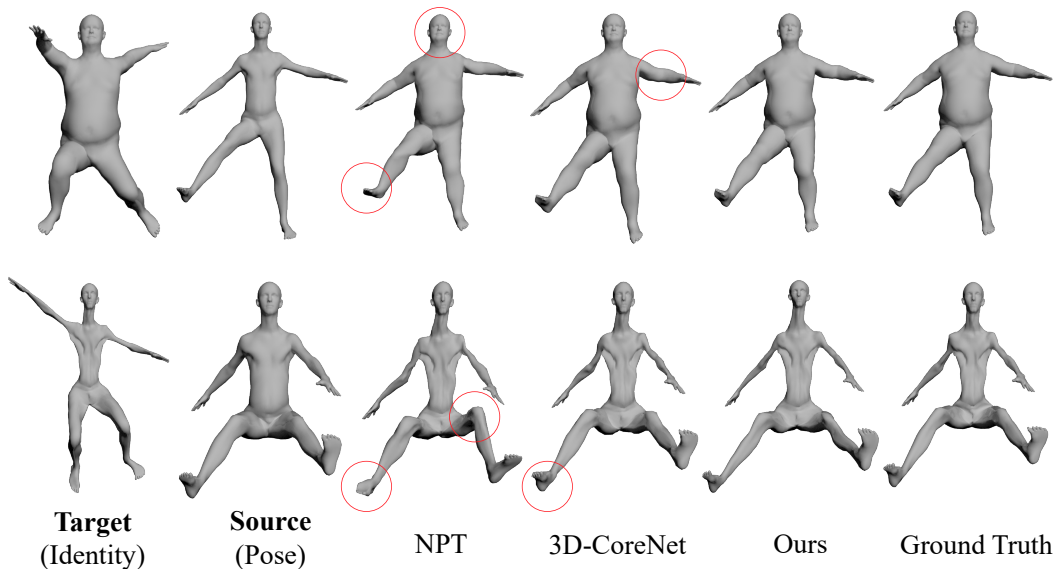


Figure 5: **Qualitative comparison of different methods on unseen human data.** The source and target meshes are from SMPL [17]. NPT produces results that are always inaccurate in head or hands and feet. 3D-CoreNet can produce similar results to our method, but the network is much larger than ours, so our method is more efficient and practical than NPT and 3D-CoreNet.

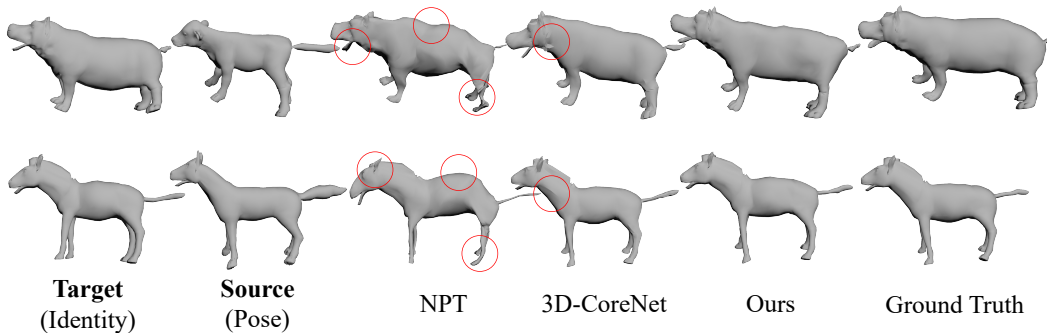


Figure 6: **Qualitative comparison of different methods for unseen animal data.** The source and target meshes are from SMAL [30]. NPT produces very flat legs and a curved torso. The results of 3D-CoreNet have local unsmooth parts. However, our method achieves better results.

4.2 Comparison with the state-of-the-arts

We choose NPT [25] and 3D-CoreNet [20] for accuracy comparison with our method. Since the NPT(origin) model lacks support for meshes with different numbers of vertices, the NPT(maxpool)

Table 1: **Quantitative comparison of average PMD.** It can be seen that our method is superior to NPT and 3D-CoreNet for different pose types of human and animal datasets.

Dataset	Pose Type	PMD↓($\times 10^{-4}$)		
		NPT [25]	3D-CoreNet [20]	Ours
SMPL [17]	Seen-pose	2.39	1.13	0.57
	Unseen-pose	8.60	4.45	1.78
SMAL [30]	Seen-pose	50.67	18.86	11.32
	Unseen-pose	70.28	25.53	17.96

model is chosen for the experiments. NPT and 3D-CoreNet only translate the center of the mesh to the origin, while our method translates the center of the mesh to the origin and then normalizes the vertex coordinates to a range of -1 to 1. Our selected validation set has different identities from the training set, which also contains seen poses and unseen poses. The PMD values of NPT, 3D-CoreNet, and our method on the validation set are recorded separately, and the qualitative comparison of these three methods is shown in Figure 5 and Figure 6, and the quantitative comparison is shown in Table 1. It can be observed that NPT and 3D-CoreNet have errors in the pose transfer for unseen poses, the foot and leg poses of NPT are not correctly transferred, and both NPT and 3D-CoreNet have significant defects in the local details, while our method preserves the local details of the mesh well and accurately transfers the poses to the target mesh. In Table 1, the PMD values of seen and unseen pose of these three methods for the two datasets are recorded, which shows that the PMD of our method is also significantly lower than NPT and 3D-CoreNet, and the size of our network is even close to NPT and much smaller than 3D-CoreNet, which also shows that the feature extraction efficiency of our method is also higher than NPT and 3D-CoreNet.

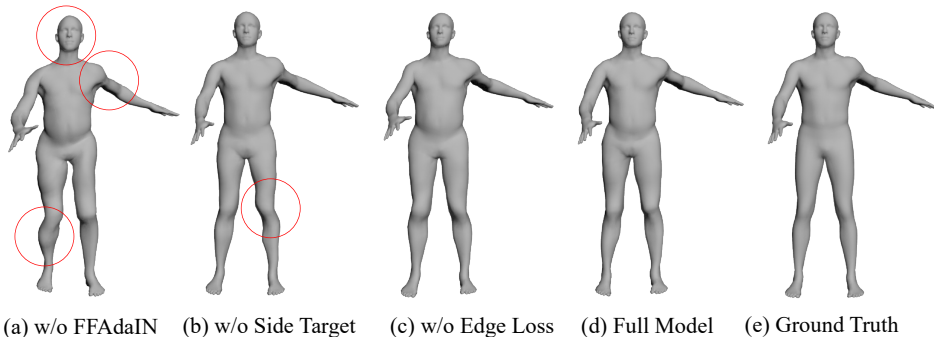


Figure 7: **Ablation study results.** When we replace FFAdaIN with SPAdaIN [25], the output mesh is distorted, and when we delete the target vertices on the side of FFAdaIN, the output is also not as good as the full model.

4.3 Ablation study

To show the key role of FFAdaIN in our method, the first variant of our method replaces the first FFAdaIN module in the forward propagation direction of the FFAdaIN ResBlock with a SPAdaIN module. Our designed FFAdaIN has the characteristic of having two side inputs, where the mixed feature input already contains the vertices of the target mesh. The reason for keeping the other separate input of the target mesh vertices is that we believe that can further refine the local details of the prediction mesh and make the prediction mesh better preserving the identity features of the target mesh. To prove this idea, the second variant of our method removes the target mesh vertices input on the side of FFAdaIN. In addition, we also designed a third variant that removes the edge length constraint loss to show the importance of edge length constraint loss. The qualitative results of the ablation study are shown in Figure 7, and the quantitative results are shown in Table 2. When replacing FFAdaIN with SPAdaIN, the output mesh appears with multiple unsmooth parts, which shows that FFAdaIN plays a key role in our method. When the target mesh vertices input on the side of FFAdaIN is removed, the effect is also not as good as the full model, which shows that FFAdaIN

Table 2: **Quantitative ablation studies of seen and unseen poses.** PMD increased significantly after replacing FFAdaIN with SPAdaIN [25]. The accuracy of the model also deteriorates when the input of the side target vertices is removed.

Pose Type	PMD↓($\times 10^{-4}$)			
	w/o FFAdaIN	w/o Side Target	w/o L_{edg}	Full model
Seen-pose	2.58	2.14	0.91	0.57
Unseen-pose	5.33	4.07	2.12	1.78

must preserve the target mesh vertices input on the side. Finally, it is shown that it can make the output mesh smoother with edge length constraints.

4.4 Generalization capability

To evaluate the generalization ability of our method, the meshes from FAUST dataset [5] and MultiGarment [4] dataset were used. The number of mesh vertices in FAUST is the same as in SMPL [17] but the human body has more identities. The number of mesh vertices in MultiGarment is larger than in SMPL and contains a complex human mesh wearing clothing. In the first group of experiments, we try to transfer the mesh pose of FAUST to the target mesh of SMPL, and in the second group, the mesh pose of SMPL is transferred to the target mesh of MultiGarment. In addition to testing the robustness of our method, in the third group, we try to apply pose transfer to the mesh of the SMPL with noise added. The results are shown in Figure 8. The first group shows that our method successfully extracts the pose features of the FAUST mesh and transfers them to the target mesh of SMPL. The second group shows that our method achieves pose transfer while preserving the local details of the target mesh well. The third group tests the robustness of our method by adding random noise within -0.05 to 0.05 to the source mesh vertex coordinates, and the results show that our method still achieves very good performance.

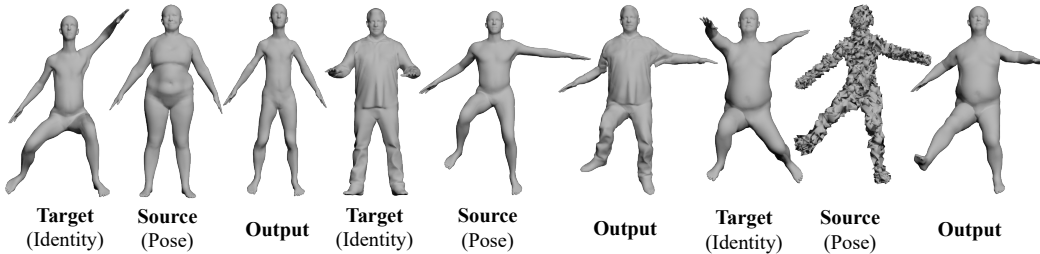


Figure 8: **Pose transfer results for the Non-SMPL human data and the human data with noise.** From left to right the first group transfers FAUST human pose to the SMPL human, the second group transfers SMPL human pose to the MultiGarment human, and the third group adds random noise to the source mesh. It can be seen that our method still has good performance.

5 Conclusion

In this paper, we propose a dual-side feature fusion 3D mesh pose transfer method (*FF-PTNet*), which solves the mesh distortion problem in lightweight method during the transfer of unseen pose, and at the same time makes the accuracy exceed past network methods. We propose the FFAdaIN module with dual-side inputs, which greatly improves the training speed of the pose transfer network and the ability to transfer unseen poses, with more computational cost savings and no additional inputs compared to other methods. In addition, our method can also be adapted to mesh pose transfer tasks with different numbers of vertices and has good robustness against noise. However, our method does not work well for some self-touching meshes. In the future, we will try to use graph networks to improve our method.

References

- [1] Tristan Aumentado-Armstrong, Stavros Tsogkas, Allan Jepson, and Sven Dickinson. Geometric disentanglement for generative latent shape models. In *Proceedings of the IEEE/CVF International Conference on Computer Vision (ICCV)*, October 2019.
- [2] Mirela Ben-Chen, Ofir Weber, and Craig Gotsman. Spatial deformation transfer. In *Proceedings of the 2009 ACM SIGGRAPH/Eurographics Symposium on Computer Animation*. ACM, aug 2009.
- [3] Paul J Besl and Neil D McKay. Method for registration of 3-d shapes. In *Sensor fusion IV: control paradigms and data structures*, volume 1611, pages 586–606. Spie, 1992.
- [4] Bharat Lal Bhatnagar, Garvita Tiwari, Christian Theobalt, and Gerard Pons-Moll. Multi-garment net: Learning to dress 3d people from images. In *Proceedings of the IEEE/CVF International Conference on Computer Vision (ICCV)*, October 2019.
- [5] Federica Bogo, Javier Romero, Matthew Loper, and Michael J Black. Faust: Dataset and evaluation for 3d mesh registration. In *Proceedings of the IEEE conference on computer vision and pattern recognition*, pages 3794–3801, 2014.
- [6] Prashanth Chandran, Gaspard Zoss, Paulo Gotardo, Markus Gross, and Derek Bradley. Adaptive convolutions for structure-aware style transfer. In *Proceedings of the IEEE/CVF conference on computer vision and pattern recognition*, pages 7972–7981, 2021.
- [7] Haoyu Chen, Hao Tang, Henglin Shi, Wei Peng, Nicu Sebe, and Guoying Zhao. Intrinsic-extrinsic preserved gans for unsupervised 3d pose transfer. In *Proceedings of the IEEE/CVF International Conference on Computer Vision*, pages 8630–8639, 2021.
- [8] Qifeng Chen and Vladlen Koltun. Photographic image synthesis with cascaded refinement networks. In *Proceedings of the IEEE international conference on computer vision*, pages 1511–1520, 2017.
- [9] Hung-Kuo Chu and Chao-Hung Lin. Example-based deformation transfer for 3d polygon models. *Journal of Information Science and Engineering*, 26(2):379–391, 2010.
- [10] Xun Huang and Serge Belongie. Arbitrary style transfer in real-time with adaptive instance normalization. In *Proceedings of the IEEE international conference on computer vision*, pages 1501–1510, 2017.
- [11] Tao Ju, Scott Schaefer, and Joe Warren. Mean value coordinates for closed triangular meshes. In *ACM SIGGRAPH 2005 Papers*. ACM, jul 2005.
- [12] Ladislav Kavan. Direct skinning methods and deformation primitives. *ACM SIGGRAPH Courses*, 2014.
- [13] Michael Kazhdan, Matthew Bolitho, and Hugues Hoppe. Poisson surface reconstruction. In *Proceedings of the fourth Eurographics symposium on Geometry processing*, volume 7, page 0, 2006.
- [14] Yuheng Li, Krishna Kumar Singh, Utkarsh Ojha, and Yong Jae Lee. Mixnmatch: Multifactor disentanglement and encoding for conditional image generation. In *Proceedings of the IEEE/CVF Conference on Computer Vision and Pattern Recognition (CVPR)*, June 2020.
- [15] Zhouyingcheng Liao, Jimei Yang, Jun Saito, Gerard Pons-Moll, and Yang Zhou. Skeleton-free pose transfer for stylized 3d characters. In *Computer Vision–ECCV 2022: 17th European Conference, Tel Aviv, Israel, October 23–27, 2022, Proceedings, Part II*, pages 640–656. Springer, 2022.
- [16] Songhua Liu, Tianwei Lin, Dongliang He, Fu Li, Meiling Wang, Xin Li, Zhengxing Sun, Qian Li, and Errui Ding. Adaattn: Revisit attention mechanism in arbitrary neural style transfer. In *Proceedings of the IEEE/CVF international conference on computer vision*, pages 6649–6658, 2021.

- [17] Matthew Loper, Naureen Mahmood, Javier Romero, Gerard Pons-Moll, and Michael J Black. Smpl: A skinned multi-person linear model. *ACM transactions on graphics (TOG)*, 34(6):1–16, 2015.
- [18] Taesung Park, Ming-Yu Liu, Ting-Chun Wang, and Jun-Yan Zhu. Semantic image synthesis with spatially-adaptive normalization. In *Proceedings of the IEEE/CVF conference on computer vision and pattern recognition*, pages 2337–2346, 2019.
- [19] Xiaojuan Qi, Qifeng Chen, Jiaya Jia, and Vladlen Koltun. Semi-parametric image synthesis. In *Proceedings of the IEEE Conference on Computer Vision and Pattern Recognition*, pages 8808–8816, 2018.
- [20] Chaoyue Song, Jiacheng Wei, Ruibo Li, Fayao Liu, and Guosheng Lin. 3d pose transfer with correspondence learning and mesh refinement. In M. Ranzato, A. Beygelzimer, Y. Dauphin, P.S. Liang, and J. Wortman Vaughan, editors, *Advances in Neural Information Processing Systems*, volume 34, pages 3108–3120. Curran Associates, Inc., 2021.
- [21] Chaoyue Song, Jiacheng Wei, Ruibo Li, Fayao Liu, and Guosheng Lin. Unsupervised 3d pose transfer with cross consistency and dual reconstruction. *IEEE Transactions on Pattern Analysis and Machine Intelligence*, pages 1–13, 2023.
- [22] Robert W. Sumner and Jovan Popović. Deformation transfer for triangle meshes. *ACM Transactions on Graphics*, 23(3):399–405, aug 2004.
- [23] Minhyuk Sung, Zhenyu Jiang, Panos Achlioptas, Niloy J. Mitra, and Leonidas J. Guibas. Deformsyncnet: Deformation transfer via synchronized shape deformation spaces. *ACM Transactions on Graphics (Proc. of SIGGRAPH Asia)*, 2020.
- [24] Dmitry Ulyanov, Andrea Vedaldi, and Victor Lempitsky. Instance normalization: The missing ingredient for fast stylization. *arXiv preprint arXiv:1607.08022*, 2016.
- [25] Jiashun Wang, Chao Wen, Yanwei Fu, Haitao Lin, Tianyun Zou, Xiangyang Xue, and Yinda Zhang. Neural pose transfer by spatially adaptive instance normalization. In *Proceedings of the IEEE/CVF conference on computer vision and pattern recognition*, pages 5831–5839, 2020.
- [26] Ting-Chun Wang, Ming-Yu Liu, Jun-Yan Zhu, Andrew Tao, Jan Kautz, and Bryan Catanzaro. High-resolution image synthesis and semantic manipulation with conditional gans. In *Proceedings of the IEEE conference on computer vision and pattern recognition*, pages 8798–8807, 2018.
- [27] Weiwei Xu, Kun Zhou, Yizhou Yu, Qifeng Tan, Qunsheng Peng, and Baining Guo. Gradient domain editing of deforming mesh sequences. *ACM Transactions on Graphics (TOG)*, 26(3):84–es, 2007.
- [28] Wang Yifan, Noam Aigerman, Vladimir G Kim, Siddhartha Chaudhuri, and Olga Sorkine-Hornung. Neural cages for detail-preserving 3d deformations. In *Proceedings of the IEEE/CVF Conference on Computer Vision and Pattern Recognition*, pages 75–83, 2020.
- [29] Peihao Zhu, Rameen Abdal, Yipeng Qin, and Peter Wonka. Sean: Image synthesis with semantic region-adaptive normalization. In *Proceedings of the IEEE/CVF Conference on Computer Vision and Pattern Recognition*, pages 5104–5113, 2020.
- [30] Silvia Zuffi, Angjoo Kanazawa, David W Jacobs, and Michael J Black. 3d menagerie: Modeling the 3d shape and pose of animals. In *Proceedings of the IEEE conference on computer vision and pattern recognition*, pages 6365–6373, 2017.